INSTITUTE OF PHYSICS PUBLISHING JOURNAL OF PHYSICS B: ATOMIC, MOLECULAR AND OPTICAL PHYSICS

J. Phys. B: At. Mol. Opt. Phys. **35** (2002) 4899–4914 PII: S0953-4075(02)54953-1

Cold collisions in a high-gradient magneto-optical trap

B Ueberholz, S Kuhr, D Frese, V Gomer and D Meschede

Institut für Angewandte Physik, Universität Bonn, Wegelerstr. 8, D-53115 Bonn, Germany

Received 18 October 2002
Published 19 November 2002
Online at stacks.iop.org/JPhysB/35/4899

Abstract

We present a detailed analysis of the cold collision measurements performed in a high-gradient magneto-optical trap with a few trapped Cs atoms first presented in Ueberholz *et al* (*J. Phys. B: At. Mol. Opt. Phys.* **33** (2000) L135). The ability to observe individual loss events allows us to identify two-body collisions that lead to the escape of only one of the colliding atoms (up to 10% of all collisional losses). Possible origins of these events are discussed here. We also observed strong modifications of the total loss rate with variations in the repumping laser intensity. This is explained by a simple semiclassical model based on optical suppression of hyperfine-changing collisions between ground-state atoms.

1. Introduction

The investigation of cold collisions of neutral atoms [1] has received much attention since the introduction of the magneto-optical trap (MOT) [2]. This device not only serves to conveniently store a large number of cold atoms at sufficiently high densities, it also serves as an energy discriminator for inelastic collisions which are typically detected through loss of stored atoms leaving the MOT only if they gain enough kinetic energy during a collision to overcome the trap recapture forces.

Cold collisions have been intensely studied in MOTs with low magnetic field gradients of order $B' = \partial B/\partial z \sim 10$ G cm^{-1}. Previous experiments performed in our group [3, 4] and at Caltech [5] have shown that the dynamics of atoms trapped in a high-gradient MOT ($B' \sim 100$–500 G cm^{-1}) is similar to that of a standard MOT. In particular, the dependence of the atomic temperature on the laser parameters is the same, because within the small trapping volume the Zeeman shift of the atomic levels is only a fraction of the natural linewidth. However, the situation for an atom *escaping* from the trap is very different. Even at relatively small displacements from the trap centre, the atomic levels are Zeeman-shifted out of resonance such that the decelerating light forces do not act efficiently. The strong magnetic field gradient reduces the recapture ability of the trap, leading to an enhanced sensitivity for low-energy products of collisional events. In particular, exoergic hyperfine-changing collisions of atoms in the ground state contribute to the total losses and are easily observable.

0953-4075/02/234899+16$30.00

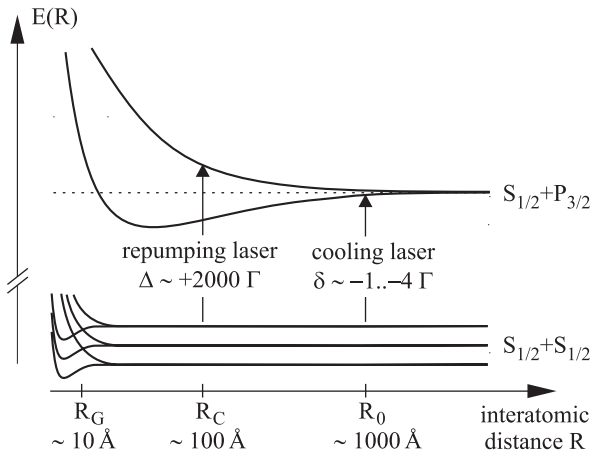

Figure 1. Schematic overview of collisional processes in a MOT. Shown are interaction energies between two atoms in the ground and excited states S + P (resonant dipole–dipole interaction $\sim \pm 1/R^3$ for large R) and two ground-state atoms S + S, F = (4, 4), (4, 3), (3, 3) (short-range interaction, essentially flat at long distances) together with distances characteristic for resonant excitation by both MOT lasers. At very short distances around R_G a change of the ground-state hyperfine structure can occur. R_C denotes the point where the repumping laser is resonant with the repulsive potential curves. The MOT cooling laser can resonantly excite the atom pair at R_0. For the heavy Cs atoms all three characteristic distances are clearly separated, thus the blue detuned repumping laser can effectively inhibit collisions between two ground-state atoms (see section 5.3).

Recently we have shown that a high-gradient MOT gives access to a novel method of cold collision studies [6]. In this system individual cold collisions can be observed in real time because the number of trapped atoms is small and can be determined exactly. Collisional loss events are identified as pairs of atoms leaving the trap. In contrast to experiments with a large number of atoms, we discriminate one-atom losses and two-atom losses with 100% efficiency. Two new effects have been observed. First, we found that a significant number of inelastic collisions leads to loss of one atom only. Second, ground-state collisions can strongly be suppressed by the repumping laser light. It is the purpose of this paper to give a full account of our observations and interpretations reported briefly in [6]. Extended analysis provides a more detailed qualitative and quantitative understanding.

2. Cold collisions in a MOT

In a MOT operated with near-resonant laser light, atoms are stored at kinetic energies near the Doppler temperature T_D given by $k_B T_D = \hbar\Gamma/2$. For Cs, the atomic natural linewidth is $\Gamma = 2\pi \times 5.22$ MHz and $T_D = 125\ \mu$K. Collisional dynamics in the presence of near-resonant laser light is governed by the long-range resonant dipole–dipole interaction. Asymptotically, the potential is of the form $V_{S+P} = \pm C_3/R^3$ for one atom in the ground and one atom in the excited state, with $C_3 \approx \hbar\Gamma[\lambda/(2\pi)]^3$. Three main exoergic collisional processes have been identified [1] and are distinguished through the origin of energy gain: radiative escape (RE), fine-structure-changing collisions (FCCs) and ground-state hyperfine-changing collisions (HCCs). The first two are light-induced processes and involve the attractive branch of the quasimolecular potential $V_{S+P} = -C_3/R^3$. The MOT cooling laser, typically red-detuned by a few natural linewidths from the cooling transition, resonantly excites an atom

pair at a separation R_0 (see figure 1). For a detuning $\delta < 0$, R_0 is given by $V_{S+P}(R_0) = \hbar\delta$. After an excitation to an attractive level the atoms are accelerated towards each other. During the collision, spontaneous emission of a photon red-shifted from the atomic resonance can take place. This so-called RE process is described by

$$A + A + \hbar\omega \rightarrow A_2^*(P_{3/2}) \rightarrow A + A + \hbar\omega' \tag{1}$$

with energy $\Delta E_{RE}/2 = \hbar(\omega - \omega')/2$ transferred to each atom. The resulting kinetic energy has a continuous distribution and the corresponding loss rate is sensitive to both the effective trap depth and the initial temperature of the stored atoms. If spontaneous emission does not occur, the atoms oscillate on the quasimolecular potential curve until they undergo a change of fine structure represented by

$$A + A + \hbar\omega \rightarrow A_2^*(P_{3/2}) \rightarrow A^*(P_{1/2}) + A + \Delta E_{FCC}, \tag{2}$$

with the energy $\Delta E_{FCC}/2$ transferred to each atom. Due to the large fine structure splitting in Cs ($\Delta E_{FCC}/2k_B = 400$ K), this process always causes an escape of both atoms from the MOT, which is usually not deeper than 1 K.

HCC processes occur at a smaller interatomic distance R_G due to the steep van der Waals potential $V_{S+S} = \pm C_6/R^6$. Atoms stored in the upper (F = 4) hyperfine state (HFS) can gain kinetic energy, because a change to F = 3 in one of the colliding atoms transfers $\Delta E_{HCC}/2k_B = 0.22$ K to each atom. If both atoms change their F quantum numbers, twice this energy is released. Thus, HCC processes will also contribute to the total loss rate if the MOT trap depth is reduced below this energy.

As we will see in the following, the atoms can also couple to a repulsive quasimolecular state by excitation with the MOT repumping laser at radius R_C (see figure 1). Here, decelerating forces can prevent atoms from reaching distances smaller than R_C where HCC processes occur. This effect will be discussed in detail in section 5.3.

3. Kinetics in a high-gradient MOT

3.1. Trap depth

Trapping of atoms in a MOT is achieved by dissipative rather than conservative forces, and the recapture ability is therefore appropriately characterized by the minimum initial kinetic energy enabling an escape, designated in the following as trap depth. Precise knowledge of the trap depth is essential for a detailed interpretation of the measurements. We numerically calculate atomic trajectories under the influence of the trapping laser field similar to [7]. The force exerted on an atom is expressed as the net absorption rate from every laser beam times the photon momentum. To determine the influence of trapping and repumping lasers, all sublevels of both ground states as well as the relevant excited states (F′ = 4, 5) are included. The populations of the various magnetic sublevels are calculated by means of rate equations. Furthermore, the strength and Zeeman shift of each transition and the Doppler shift for every laser beam are explicitly taken into account. By projecting all laser beams onto the quantization axis determined by the local magnetic field $\vec{B}$ at every point of the trajectory, we account for the three-dimensionality of the problem.

In figure 2(a) we show the calculated trap depth as a function of the field gradient for typical cooling laser detunings δ. Here $s_0 = I/I_0$, with saturation intensity $I_0 = 1.1$ mW cm^{-2} and total cooling laser intensity I. Note that with increasing B' the trap depth first increases to a maximum value and falls off again. For a homogeneous beam profile the maximum trap depth is obtained at a magnetic field gradient $B'_\delta \approx \hbar\delta/(\mu_B r_{beam})$ where the Zeeman shift at beam radius r_{beam} compensates the detuning δ of the cooling laser, with μ_B as the Bohr magneton.

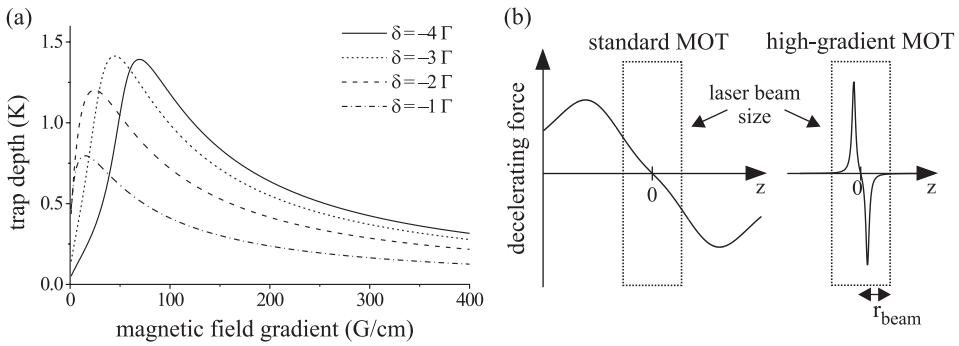

Figure 2. Comparison of a standard MOT with a high-gradient MOT. (a) Calculated trap depth as a function of the magnetic field gradient, for cooling laser saturation parameter $s_0 = 80$, beam radius $r_{\text{beam}} = 2$ mm and different cooling laser detunings δ. (b) Decelerating force (as a sum of two Lorentzian profiles from two counterpropagating beams) shown for slow atoms and spatially constant laser intensities. In a standard MOT the recapture ability is limited by the finite laser beam size, whereas in a high-gradient MOT the atoms are Zeeman-shifted out of resonance within the laser beams.

The reason for this behaviour is qualitatively explained in figure 2(b). The decelerating force acting on an escaping atom is spatially dependent due to the Zeeman effect and the intensity profile of the laser beam. In a standard MOT with moderate field gradients the size of the laser beam mainly determines the extent of the region in which atoms can be decelerated. An increase of the magnetic field gradient leads to a larger decelerating light force and thus to a deeper trap. In a high-gradient MOT, however, the maximum (resonant) value of the light force is already achieved within the laser beam and a further increase in B' will only shorten the decelerating distance, reducing the recapture ability of the trap. This will manifest itself, in our case, in overall higher collisional loss rates, as will be shown in section 5.1. To obtain a reasonable loading rate, the absolute value of the cooling laser detuning has to be increased to several natural linewidths.

3.2. Temperature of stored atoms

Cold collisions in a MOT are also affected by the initial kinetic energy defining the flux into each loss channel. Within the Doppler cooling theory [8] the light force in the centre of the MOT can be described by $\mathrm{F} = -\kappa z - \alpha \dot{z} - \xi(t)$. Here κ is the MOT spring constant proportional to B' and α is the damping coefficient. The fluctuating Langevin force $\xi(t)$ accounts for the stochastic nature of photon absorption and emission and is responsible for heating processes. In the simple case of a two-level atom moving in a standing wave of σ^+–σ^- counterpropagating laser beams (1D MOT configuration) of low intensity, the Doppler theory predicts that dissipative forces dominate at the trap centre in a high-gradient MOT, whereas at small displacements from the centre (a few micrometres) restoring forces can become dominant and may even dominate over a wide part of the trap volume.

Using the equipartition theorem, the temperature in a Cs MOT is usually approximated by

$$T \approx \frac{\Gamma}{|\delta|} \frac{B'}{[1\ \mathrm{G\ cm^{-1}}]} \frac{r_0^2}{2k_{\mathrm{B}}} \times 10^{-19}\ \mathrm{N\ m^{-1}} \tag{3}$$

for low cooling laser intensities ($s_0 < 1$) and detunings $|\delta| > 2\Gamma$ [9, 10]. In our intensity regime ($s_0 > 10$) the trap was observed to have a Gaussian envelope with size r_0 proportional

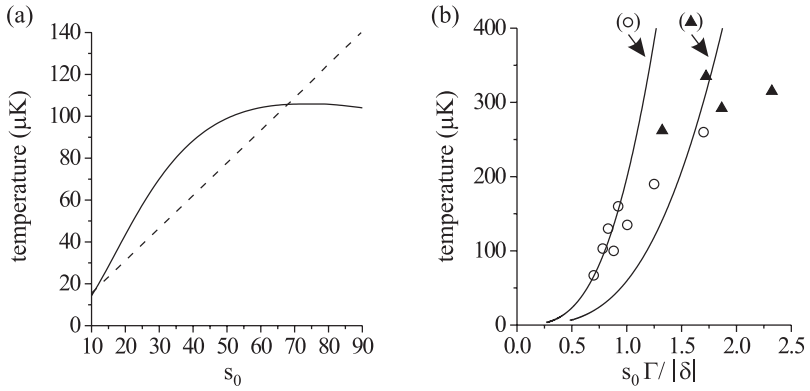

Figure 3. (a) Temperature in our MOT as a function of cooling laser saturation parameter s_0 with observed trap size $r_0 \approx 2.0\ \mu\text{m} \times \sqrt{s_0}$ for detuning $\delta = -3.35\Gamma$ and $B' = 375\ \text{G cm}^{-1}$ (solid curve). The dashed line shows the dependence according to equation (3). (b) Comparison of our calculations (solid curves, without fitting) with experimental data from a high-gradient MOT (atom number $N \approx 10^4$) at $B' = 92\ \text{G cm}^{-1}$ with varying detuning δ [4], plotted as a function of light-shift parameter $s_0\Gamma/|\delta|$ (circles: $s_0 = 2$, triangles: $s_0 = 3.6$).

to $\sqrt{s_0}$, as expected for a gas with a Maxwell–Boltzmann velocity distribution confined in a harmonic potential. In figure 3(a) we show the temperatures given by equation (3) (dashed line). For low intensities and high detunings this is the same temperature dependence found experimentally [9] and theoretically [11] for a Cs 3D σ^+–σ^- optical molasses and was also adequately confirmed in the Caltech group for a high-gradient MOT [5]. However, as experimental results show, the linear dependence fails if the effective saturation parameter for total laser intensity reaches $s = s_0/[1 + (2\delta/\Gamma)^2] \approx 1$.

To account for the high laser intensities used in our experiment, we use a temperature estimation by means of a semiclassical model similar to trap depth calculations. Here we assume that the atoms are decelerated by the light force from the trap centre with initial kinetic energy $k_B T_r$ up to the edge of the MOT with the measured trap radius r_0. For simplicity, we use a fictitious atom with a $J = 0 \rightarrow J' = 1$ transition in counterpropagating σ^+–σ^- laser beams [12]. In this model no restrictions are made for the light field intensity and for the velocity (temperature) of the atoms. Since the cooling cycle can be treated as closed within the MOT volume we neglect repumping transition states. As shown in our previous work [16], stored atoms in our MOT are pumped into the states maximally coupled to the light field which supports the used model. Furthermore, sub-Doppler theory is known to fail for intensities above $s_0 > 1$ and nonzero magnetic fields [13] and thus we ignore wavelength-scale polarization gradients.

The results of our calculations are shown in figure 3(a) (solid curve). The temperatures given by equation (3) are similar for lower intensities, whereas for values above $s_0 \approx 50$ (corresponding to $s \approx 1$) the temperature reaches a finite value, as one would expect for a two-level atom due to power broadening of the cooling transition. In fact, such a qualitative behaviour, i.e. the deviation from the linear dependence of the temperatures with increasing laser intensity, has also been observed in a Cs optical molasses [9] and a standard Rb MOT [14] as the effective saturation parameter reaches $s \approx 1$. To manifest our temperature calculation we applied this model to trap parameters of a high-gradient MOT [4] with a larger number of atoms. Here, we found good agreement with measured temperatures for detunings $|\delta| > 2\Gamma$, at which κ was found to be independent of laser intensity [10] (see figure 3(b)). In particular,

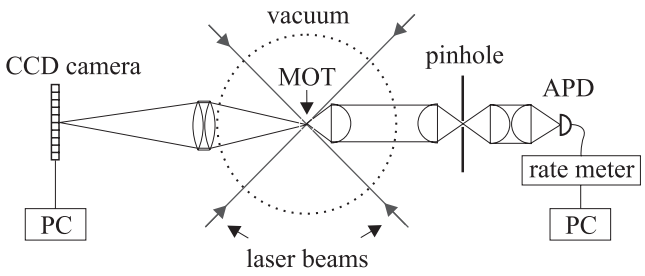

Figure 4. Schematic diagram of the experimental setup. On the left, a CCD camera monitors the spatial distribution of the fluorescing atoms stored in the trap. Time-resolved photon detection is achieved by a 1:1 imaging onto an APD, where a pinhole filters stray light.

the model yields a qualitatively more realistic dependence of T from $\Gamma/|\delta|$ than the linear dependence of equation (3).

4. Experiment

Our experimental setup has been described in detail elsewhere [15–17]. A six-beam σ^+–σ^- MOT is loaded from low-pressure Cs vapour. The magnetic quadrupole field of $B' = 375\,\mathrm{G\,cm^{-1}}$ is produced by permanent magnetic discs. Diode lasers are used to provide cooling and repumping laser beams. The detuning of the cooling laser from the $\mathrm{F} = 4 \rightarrow \mathrm{F}' = 5$ transition is controlled via heterodyne phase locking to a reference laser. For depopulation of the lower ground state the repumping laser is stabilized by polarization spectroscopy to the $\mathrm{F} = 3 \rightarrow \mathrm{F}' = 4$ transition with linewidth less than 1 MHz. It is superimposed onto the cooling laser beams in two $(x + y)$ of the three MOT axes. The laser beams are apertured to a beam radius of $r_{\mathrm{beam}} = 2$ mm. The saturation parameter of the cooling laser can be varied between $s_0 = 12$ and 115. The lower limit of s_0 is caused by the rapidly dropping loading rate such that the MOT dynamics becomes too slow. Fluorescence from the atoms is imaged onto two opposite detectors in the x–y plane at an angle of 45° with respect to the laser beams, see figure 4. On the one side the MOT is imaged onto a CCD camera to measure the spatial distribution of the atoms. The $1/e^2$ radius r_0 of the trap is in the range of 7–24 μm depending on the detuning and intensity of the cooling laser. The trap size was observed to be independent of the atom number (up to $N = 8$) ensuring that radiation trapping effects [18] can be ignored. Fluorescence photons are also detected by an avalanche photodiode (APD) with a detection efficiency of 50% at $\lambda = 852$ nm. The APD is cooled to $-10\,^{\circ}\mathrm{C}$ to reduce its dark count rate below $15\,\mathrm{s^{-1}}$. A lens mounted inside the vacuum chamber collects the fluorescence light from a solid angle of 4%. Typical photon count rates are $(3\text{–}20) \times 10^3\,\mathrm{s^{-1}}$/atom depending on the cooling laser detuning and intensity.

The photon counts are integrated within time intervals of $t_{\mathrm{I}} = 100$ ms and recorded for many hours at constant trap parameters. A typical sequence is shown in figure 5. We directly resolve the temporal evolution of the atom number $N(t)$ in the trap, limited to an atom number $N < 20$ by the signal-to-noise ratio. A computer program digitizes the signal $N(t)$ and extracts the desired information on the collisional statistics. The probability for misinterpretations (for example two one-atom losses occurring simultaneously within t_{I} being detected as a two-atom loss event) is below 1% and can be neglected.

In experiments with many atoms the dynamics of the atom number N obeys the rate equation

$$\dot{N} = R - N/\tau_{\mathrm{c}} - \beta \int n^2(\boldsymbol{r}, t)\,\mathrm{d}^3 r. \tag{4}$$

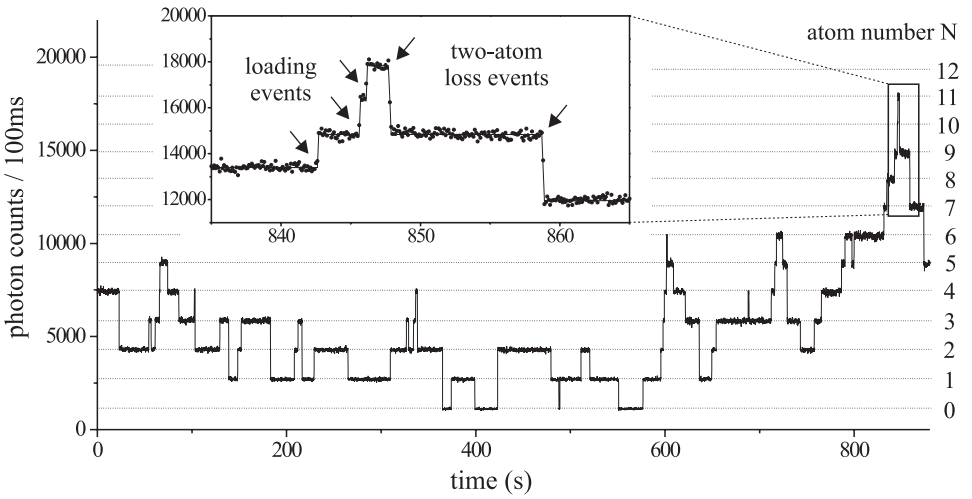

Figure 5. Excerpt from a typical fluorescence signal detected with an APD. The integration time for each point is $t_I = 100$ ms. The count rate for $N = 0$ is caused by residual stray light. Inset: enlarged section with separate loading and loss events together with the discretized signal (straight line) used for the determination of the loss rates. The arrows mark a change in the number N of stored atoms.

Atoms are loaded at random from the background atomic vapour at rate R or are removed from the trap by collisions with background gas at rate $1/\tau_c$. Due to the inelastic cold collisions described above, atom pairs can leave the trap. Knowing the temporal evolution of the trapped atom number $N(t)$ and their density profile $n(\boldsymbol{r}, t)$, the total rate coefficient β ($[\beta] = \mathrm{cm}^3\ \mathrm{s}^{-1}$) for cold collisions can be derived. However, radiative trapping effects (typically for atom numbers $N > 10^6$) may change the density profile and much effort is needed to precisely determine the absolute atom number $N(t)$.

In our experiment the exact number of trapped atoms is known which allows us to distinguish separate loading and loss events. This leads to the following rate equation with two loss rates $L_{1\mathrm{atom}}$ and $L_{2\mathrm{atoms}}$ for one and two atoms respectively:

$$\dot{N} = R - L_{1\mathrm{atom}} - 2L_{2\mathrm{atoms}}. \tag{5}$$

Figure 6 shows the measured loading and loss event rates as a function of the atom number N. We observed no change of the loading rate R with N, and $L_{2\mathrm{atoms}}$ shows a dependence proportional to $N(N-1)$ as expected. If one-atom losses are assumed to result from collisions with background-gas atoms only, $L_{1\mathrm{atom}}$ should depend linearly on the atom number (see appendix for details).

Astoundingly, a quadratic increase of the one-atom loss rate has been observed. Possible explanations for this observation will be discussed in section 5.4. The occurrence of the quadratic one-atom loss rate leads to the following equations that connect $L_{1\mathrm{atom}}$ and $L_{2\mathrm{atoms}}$ with the corresponding rate coefficients β_1 and β_2:

$$L_{1\mathrm{atom}} = N/\tau_c + \beta_1 \frac{N(N-1)}{V}, \qquad L_{2\mathrm{atoms}} = \frac{\beta_2}{2}\frac{N(N-1)}{V}. \tag{6}$$

V is defined by the peak density volume V_p of the Gaussian sphere,

$$V = 2^{3/2} V_p \qquad \text{with } V_p = \int_0^\infty \frac{n(\vec{r})}{n(0)}\, \mathrm{d}^3 r = \left(\frac{\pi}{2}\right)^{3/2} r_0^3. \tag{7}$$

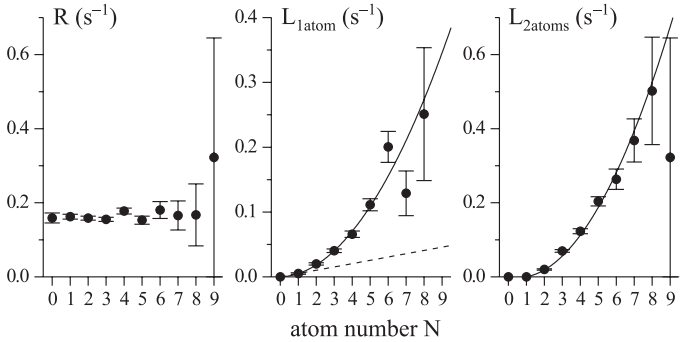

Figure 6. Loading rate (R), one-atom loss rate ($L_{1\mathrm{atom}}$) and two-atom loss rate ($L_{2\mathrm{atoms}}$) versus atom number N. The average atom number during the measurement was $\langle N\rangle = 2.6$. Cooling laser parameters are $s_0 = 38$, $\delta = -3.35\Gamma$. Solid curves represent a second-order polynomial fit. The dashed line shows a linear extrapolation of $L_{1\mathrm{atom}}$ for $N = 1$ due to background-gas collisions only. Note that $L_{1\mathrm{atom}}$ also shows a quadratic increase.

From equations (5) and (6) we derive the rate equation for small atom numbers that includes the total loss coefficient $\beta = \beta_1 + \beta_2$,

$$\dot{N} = R - N/\tau_c - \beta\frac{N(N-1)}{V}. \tag{8}$$

Note that errors for measurements of β are only given by the number of loss events and by the uncertainty of the trap size r_0.

5. Results and discussion

5.1. Cooling laser dependence

Monitoring β as a function of the cooling laser intensity is a standard measurement in cold collision studies. The first experiment of this kind was carried out by Sesko *et al* [19] for a standard Cs MOT. The intensity dependence shown in figure 7(a) (circles) was observed, with a rate constant decreasing rapidly from $\beta \approx 8 \times 10^{-11}$ cm^3 s^{-1} at low intensities to $\beta \approx 3 \times 10^{-12}$ cm^3 s^{-1} at $s = 0.7$, followed by a linear increase at higher intensities.

This characteristic minimum in the intensity dependence of β was also observed for other alkalis in standard MOTs [1] and is usually explained in the following way. With increasing cooling laser intensity the trap depth eventually exceeds the value of ΔE_{HCC} and closes this loss channel. With further increasing intensity light-induced losses play the dominant role leading to a loss rate roughly proportional to the laser intensity. Alternatively, Telles *et al* [20] attribute the increase of β with lower intensities to RE processes only. If with decreasing intensity the trap depth falls off faster than the average energy released by RE processes an increase of the loss rates can occur. However, we have carefully studied this case for our parameters but did only find an increase of the RE loss rates for intensities below $s < 0.1$ which is far apart from the parameter range relevant for our experiment.

In our MOT, strong field gradients strongly reduce the trap depth even at large intensities. Hence HCC processes always contribute to the loss rate and no minimum is observed (figure 7(a), squares). This situation has also been observed and discussed in [7] for a Rb MOT at large cooling laser detunings when the trap is sufficiently shallow.

The overall higher collisional loss rate in our measurements in comparison to standard MOTs is partially due to a larger contribution of RE losses caused by a lower trap depth as

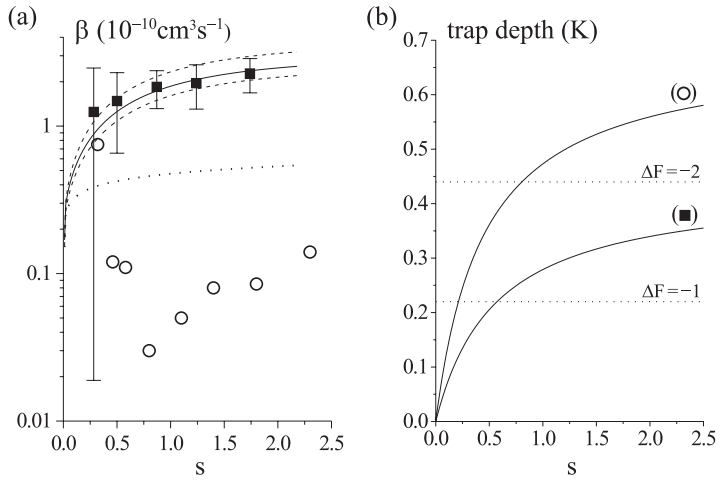

Figure 7. (a) Loss coefficient β as a function of the cooling laser saturation parameter s. Shown are our results (squares, for $\delta = -3.35\Gamma$ and repumping laser saturation parameter $s_r = 4$) together with those performed in a standard Cs MOT [19] (circles). The solid curve is a fit to our data using the GPM. Dashed curves show its uncertainty due to changes in the trap depth by a factor of 2. The dotted curve represents the losses due to HCC processes derived in section 5.3. (b) Calculated trap depths for both experiments denoted as in (a). The dotted lines show the collisional excess energies for one or two spin-flips in a HCC process (see text).

explained in [6]. To support this interpretation, we used the numerical model presented above to calculate the trap depth for the parameter in [19] ($B' = 5$ G cm^{-1}, $\delta = -1\Gamma$ and Gaussian beam profile with $r_{\mathrm{HWHM}} = 2.5$ mm) as well as for our parameters, see figure 7(b). Both curves show the same qualitative behaviour, but for our case of high B' the trap depth is nearly half that in the standard MOT [19]. However, the calculated trap depth still remains slightly above 0.22 K. Our model might overestimate the trap depth of the standard MOT, because below $s = 0.7$ the trap depth should decrease below 0.22 K. This may indicate that either the model is not sufficiently sophisticated or the released energy is mainly due to $\Delta F = -2$ HCC processes.

However, we calculated the expected light-induced loss coefficients for RE and FCCs using the simple model by Gallagher and Pritchard (GPM) [1, 21] and made some extensions to the model compared to our previous work [6]. In particular, we included both the trap depth and the atomic velocity distribution in our calculations. Furthermore, we introduced the loss coefficient β_{HCC} for HCC processes as a temperature-dependent offset to the light-induced losses.

The result for the total collisional loss coefficient is shown in figure 7(a) (solid curve). The dotted curve is a fit of β_{HCC} to experimental data, which we discuss later in section 5.3. By scaling the loss coefficient for RE and FCCs with a factor of 5.1 we find good agreement with our data. For the FCC processes we used a transition probability $P_{\mathrm{J}} = 0.035$ as an average over all relevant entrance channels [22]. Here, the RE losses were found to be about twice the FCC losses which let us assume that RE is the dominant loss process in our trap. Note that the model is known to yield the expected loss coefficients qualitatively rather than in a quantitative manner [1]. However, due to the simplifications made in this model, the results are quite reasonable and we find consistency with the scaling factor of 4.5 for light-induced processes as found for the standard Cs MOT [23].

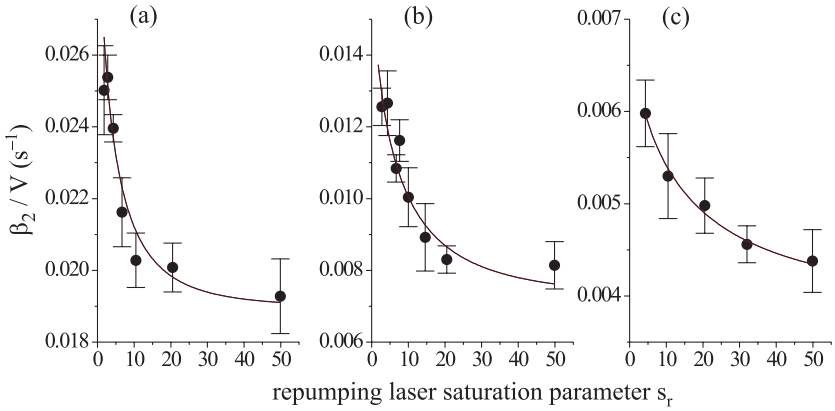

Figure 8. Loss rate β_2/V as a function of repumping laser saturation parameter $s_r = I_r/I_0$ for different trap parameters. (a) $s_0 = 40$, $\delta = -3.35\Gamma$; (b) $s_0 = 80$, $\delta = -3.35\Gamma$; (c) $s_0 = 115$, $\delta = -2.3\Gamma$. The solid curves are plots according to equation (15). The resulted fit parameters T are given in table 1.

5.2. Repumping laser dependence

The repumping laser is usually not taken into account in cold collision studies. Although needed for a normal MOT operation, its exact parameters are not very critical for the MOT performance. On average only after 10^4 cooling cycles does an atom decay into the lower HFS and has to be pumped back into the cooling cycle. The corresponding repumping time only has to be sufficiently shorter than the typical diffusion time of the atom through the trap volume (milliseconds). This is easily achieved for a large range of repumping laser intensities. In our experiment, however, we have observed a strong dependence of the losses on the repumping laser intensity, first presented in [6].

We observed a decrease of the total loss rate to a constant offset with increasing repumping laser intensity I_r, see figure 8. For all trap parameters, we found the same qualitative behaviour but with different decay constants and offsets. The maximum change in the loss rate is up to 30%. Note that in figure 8 we plotted the loss rate β_2/V instead of the loss coefficient β_2, to disregard the large error in V. This is justified since the trap size is independent of s_r.

Before we discuss the underlying mechanism, we will exclude two alternative explanations of the observed effect. First, the trap depth does not significantly change due to variations of the repumping laser intensity (see figure 9). The trap depths are essentially independent (at most 7% change) of the repumping laser intensities used for measurements in figure 8. Such small variations of the trap depth cannot influence FCCs and HCCs with their fixed values of the released energy. We also calculated the dependence of the RE loss rate as a function of the trap depth by means of the GPM. The model predicts that the RE collisional loss rate should only decrease by about 3% for our trap parameter range. Neither the variation of the decay constants nor the absolute reduction of the loss rate can be explained by this model.

In principle, it is also possible that the products of an HCC ending in the F = 3 ground state are sensitive to the repumping laser intensity. An escaping atom has to be repumped into the cooling cycle before it feels the decelerating light force again. This effect has been discussed and indeed observed in [7] but at much lower repumping laser intensities. The Doppler shift for an atom at $E_{kin} = k_B \times 0.22$ K is 1.2Γ. Since the repumping laser is exactly at resonance and the saturation parameter is still well above 1, the repumping time is of the order of several natural lifetimes $1/\Gamma$. For our parameters, this time can be completely neglected compared

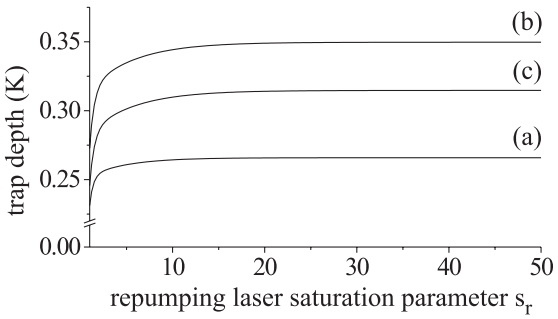

Figure 9. Calculated trap depth as a function of repumping laser saturation parameter s_r. The parameters for the curves (a), (b) and (c) relate to figure 8.

to the time the atom needs to escape from the trap, which is of the order of some tens of microseconds, ruling out this effect to account for the observed reduction of the loss rate.

5.3. Optical suppression by the repumping laser field

Light fields can not only facilitate inelastic collisions by exciting atom pairs to long-range attractive molecular potentials, they can also modify atomic interactions such that collision partners are prevented from close encounters. This phenomenon is called *optical shielding* and was studied by several groups [24–28]. In a simple semiclassical picture (see figure 1) both atoms, initially in the ground state, approach on the S + S potential curve. At the Condon radius R_C a laser detuned by Δ to the blue becomes resonant with a repulsive molecular state. The atoms are excited and repel each other before they reach a distance $R_G < R_C$ where a change of the hyperfine ground state occurs. This leads to a suppression of inelastic ground-state collisions.

A more complete description of the dynamics of this process is obtained in the dressed-atom picture (see figure 10(a)). If the atomic motion is again treated classically, the internal quantum states of the system are represented in a product basis of atomic and field states. In this basis the two relevant states $|S + S, n_\gamma\rangle$ and $|S + P, n_\gamma - 1\rangle$ are energetically degenerate at R_C (dotted lines in figure 10(a)). The coupling of these levels causes a Rabi splitting of $\hbar\Omega$ at R_C. If the atoms approach, the system can adiabatically follow the upper repulsive potential curve, or undergo a transition to the lower-lying curve. The transition probability is given by the Landau–Zener formula [29],

$$P_{LZ} = \exp\left(-\frac{\pi\hbar\Omega^2}{2Dv_C}\right), \tag{9}$$

where

$$D = \left|\frac{\partial V_{S+S}}{\partial R} - \frac{\partial V_{S+P}}{\partial R}\right|_{R_C} \approx \frac{3C_3}{R_C^4} \tag{10}$$

is the difference of the slopes of the potential curves and v_C the relative velocity of the colliding partners at R_C. The Rabi frequency is expressed as a function of s_r as $\Omega = 1/\sqrt{3} \times \sqrt{s_r/2} \times \Gamma$. The factor of $1/\sqrt{3}$ results from directional averaging of the collision axis relative to the polarization vector of the laser light [30].

If a diabatic transition occurs, the atoms approach more closely and a change of the HFS can occur with probability η. If an HFS collision does not take place, the atoms separate and

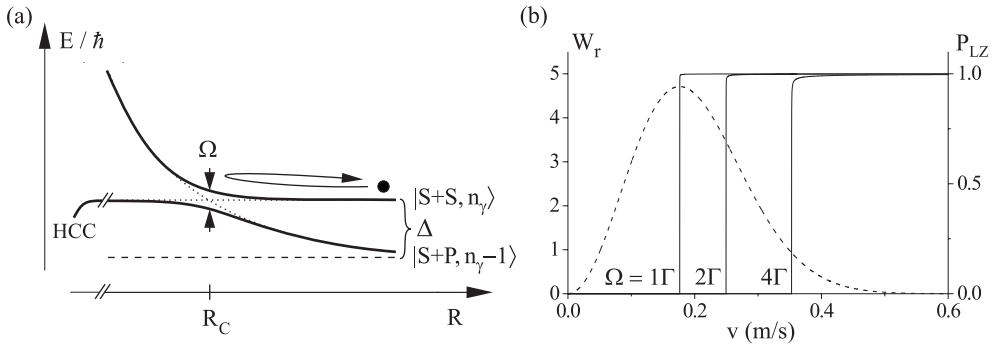

Figure 10. (a) Optical suppression in the dressed-atom picture. Slow atoms are prevented from reaching the inner regions where HCC processes can occur. The process is treated as a Landau–Zener-avoided crossing with Rabi splitting Ω at Condon radius R_C, adapted from [1, 25]. (b) Maxwell–Boltzmann distribution $\mathcal{W}_r$ (dashed curve, for $T = T_D$) and Landau–Zener transition probability P_{LZ} as a function of the relative velocity v between two colliding atoms. The fraction of atoms with velocities where $P_{LZ} \approx 1$ contributes to HCC processes.

reach the Condon point again. A following of the lower potential curve, which requires another transition, would lead to an energy transfer of $E_{kin} \approx \hbar\Delta$ to the atoms.

Note that at first sight it is impossible to discriminate these light-induced inelastic collisions from $\Delta F = -1$ HCC processes, since the released energies are approximately equal. For an atom pair reaching R_C, the loss probability P_{loss} is

$$P_{loss} = \eta P_{LZ} + P_{LZ}(1-\eta)(1-P_{LZ}) + (1-P_{LZ})P_{LZ}, \tag{11}$$

which can be rewritten as

$$\begin{aligned} P_{loss} &= \eta P_{LZ} + (2-\eta)P_{LZ}(1-P_{LZ}) \\ &\equiv P_{HCC} + P_{ind}. \end{aligned} \tag{12}$$

However, we shall see below, that P_{LZ} is either 1 or 0 and thus induced losses with probability $P_{ind} \propto P_{LZ}(1-P_{LZ})$ can be neglected. The MOT repumping laser is blue-detuned by $\Delta = (9.19 - 0.25)$ GHz $= 8.94$ GHz due to the difference in hyperfine splitting between the cooling and repumping transitions. For typical repumping laser intensities the Rabi splitting Ω is of the order of several Γ. To reach R_C, the atom pairs must have a kinetic energy of half that splitting. If the temperature of the MOT is near the Doppler temperature $T_D = \hbar\Gamma/2$, a significant number of the colliding atoms will be reflected before a collision will take place. Integration over the Maxwell–Boltzmann distribution $\mathcal{W}_r$ of relative velocities v yields the observable total loss probability,

$$P_S(s_r, T) = \int_{v_{min}}^{\infty} P_{loss}(v_C(v, s_r))\mathcal{W}_r(v, T)\,dv, \tag{13}$$

with

$$\mathcal{W}_r\,dv = \frac{4}{\sqrt{\pi}}\frac{v^2}{\tilde{v}^3}\exp\left(-\frac{v^2}{\tilde{v}^2}\right)dv, \tag{14}$$

where $\tilde{v} = \sqrt{2k_BT/\mu}$ is the relative velocity at temperature T and $\mu = m/2$ is the reduced mass. The velocity $v_C(v, s_r)$ in the Condon point depends on the repumping laser saturation parameter s_r and the initial velocity v which is derived from energy conservation, $v_C(v, s_r) = \sqrt{v^2 - \hbar\Omega/\mu}$. From $v_C(v_{min}, s_r) = 0$ the lower integration limit in equation (13) is given by $v_{min} = \sqrt{\hbar\Omega/\mu}$. For the evaluation of equation (13) one has to calculate the

Table 1. Experimental results of optical suppression of cold collisions by the repumping laser field. The temperatures T are fitting parameters from figure 8. T_r is the temperature extracted from the calculations (see section 3.2). s_0, δ and r_0 correspond to the cooling laser saturation parameter, detuning and trap size respectively.

s_0	δ (Γ)	r_0 (μm)	β_{LI} (10^{-10} cm^3 s^{-1})	β^0_{HCC} (10^{-10} cm^3 s^{-1})	T (μK)	T_r (μK)
40	−3.35	11.1 ± 1.1	1.46 ± 0.43	1.10 ± 0.43	62 ± 19	89 ± 23
80	−3.35	14.8 ± 1.2	1.30 ± 0.37	1.78 ± 0.55	84 ± 27	106 ± 28
115	−2.3	23.7 ± 1.0	2.90 ± 0.97	2.32 ± 0.69	127 ± 126	113 ± 10

transition probability P_{LZ} for different intensities of the repumping laser (see figure 10(b)). For all relevant parameters, P_{LZ} shows a step-like shape. Due to the strong exponential dependence in equation (9), P_{LZ} rises from 0 to nearly 1 within a small velocity interval Δv. Expressed in terms of the characteristic atomic velocity in the trap v_D at T_D, $\Delta v < 10^{-2} v_D$ for $\Omega < 4\Gamma$ and $P_{LZ} = 0.95$. Thus, the atoms are divided into two velocity classes. Slow atoms ($v < v_{min}$) are deflected before they reach the crossing point, whereas atoms with enough kinetic energy ($v > v_{min}$) pass through the crossing point diabatically. They approach more closely and possibly undergo a change of HFS.

The induced losses are negligible in equation (12), since the interaction region becomes very narrow due to the steep potential curves at $R_C \approx 100$ Å. The resulting interaction time is of the order of 0.1 ns which is much smaller than the excitation time $\pi/\Gamma\sqrt{6/s_r} \approx 230\,\text{ns}/\sqrt{s_r}$.

Assuming $P_{LZ} = 1$ for $v > v_{min}$, then we rewrite equation (13) as

$$P_S(s_r, T) = \eta\left[\frac{2}{\pi}\rho e^{-\rho^2} - \text{erf}(\rho) + 1\right] \qquad \text{with } \rho \equiv \frac{v_{min}}{\tilde{v}} = \sqrt{\frac{T_D}{T}\frac{\Omega(s_r)}{\Gamma}}. \tag{15}$$

Note that the observed loss probability P_S should only depend on the ratio of $\Omega(s_r)/T$. Varying T changes the fraction of atoms which contribute to HCC losses as can be seen in figure 10(b). In figure 8 we showed theoretical predictions according to equation (15) with temperature T as the only fit parameter varying P_S with s_r.

At high repumping laser intensities HCCs are totally suppressed and the contributions of light-induced losses β_{LI} (RE + FCC) remain constant. This allows us to extrapolate β_{HCC} for the three curves in figure 8 for $s_r \to 0$, denoted as β^0_{HCC}. The results for loss coefficients and temperature are presented in table 1. A comparison with the expected temperatures T_r derived in section 3.2 shows a good agreement within our model.

Finally, we want to give a crude estimation of the transition probability η for HCC processes using the semiclassical Langevin model [31]. By setting the collisional rate coefficient of non-shielded ground-state atoms equal to the Langevin capture rate coefficient times η we obtain

$$\beta^0_{HCC} = \eta\frac{9\pi}{4}\sqrt{\frac{3k_BT}{\mu}}\left(\frac{6C_6}{k_BT}\right)^{1/3}, \tag{16}$$

where $C_6 = 4340$ eV Å^6 is the van der Waals coefficient for two ground-state Cs atoms [32]. A value of $\eta = 0.59 \pm 0.11$ fits to our data which agrees reasonably well with the estimated value of 0.3 determined in a standard Cs MOT [23], taking into account that the presence of the repumping laser field partially reduces HCC losses and thus may underestimate η. In particular, we found a suppression factor of about $\beta_{HCC} \approx 1/3\beta^0_{HCC}$ for our collision measurements with varying cooling laser intensity at a constant repumping laser saturation parameter $s_r = 4$, yielding the HCC loss coefficient as shown by the dotted curve in figure 7(a).

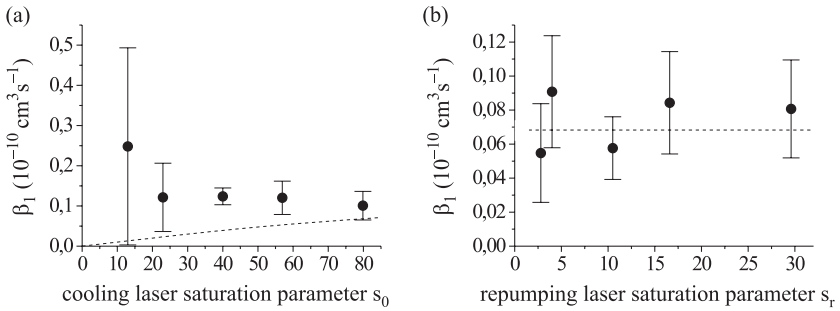

Figure 11. Summary of measurements of the quadratic one-atom loss coefficient β_1. The cooling laser detuning was fixed at $\delta = -3.35\Gamma$. (a) Variation of cooling laser intensity at constant repumping laser saturation parameter $s_r = 4$. (b) Variation of repumping laser intensity at fixed cooling laser saturation parameter $s_0 = 80$. The dashed curves show the predictions of the RE loss coefficient β_{RE} due to the asymmetric uncertainties in the trap depth (see text).

5.4. Cold collisions with one-atom loss

The unique ability to directly observe and to distinguish between one- and two-atom loss events allows us to identify two-body collisions between trapped atoms that lead to the departure of only one atom (see figure 6). Up to 10% of the observed cold collision losses are two-body-induced one-atom losses. Despite a careful analysis of the possible origins presented below, this effect still remains puzzling.

An inelastic collision of two cold atoms of equal mass and nearly at rest in a MOT is highly symmetric. As a result of a collision, both atoms leave the trap in opposite directions with nearly identical velocities. The kinetic energy of the atoms before a collision is of the order of about 100 μK and can be neglected. Not only is the gained energy equally divided between both escaping atoms but also the MOT configuration is symmetric with respect to the axis defined by the direction of motion. The production of a one-atom loss requires an energy gain comparable to the effective trap depth. This immediately excludes large-energy FCC processes as a possible loss channel. Furthermore, there is no obvious variation of the one-atom loss rate β_1 with cooling laser intensity nor with repumping laser intensity (see figure 11).

Thus we conjecture that ground-state HCCs can be ruled out because they, in contrast, show a strong dependence on the repumping laser intensity as described above. Also, the exact location of the collision in an anisotropic MOT cannot be very critical for the subsequent recapturing process. The maximum difference in the trap depth for two atoms starting their escape in the outermost region of the MOT volume or at the MOT centre was calculated to be less than 3% but can be neglected on average. Furthermore, the intensity imbalance of the counterpropagating beams, which can be measured precisely, does not change the effective trap depth significantly.

We suggest that one-atom losses are products of RE processes only. Most of the energies ΔE_{RE} released by RE processes are of the order of the trap depth because the distribution of ΔE_{RE} falls off faster than exponentially with increasing energies. One possible mechanism breaking the symmetry of the collision process could be optical pumping during a slow cold collision. For simplicity, let us suppose there are two atoms in the same outermost Zeeman state $m_F = 4$ after a collision. In order to be recaptured, one atom has to be decelerated by a σ^+-polarized laser beam while the second one will be slowed by the counterpropagating σ^--polarized beam. Due to the very different coupling strengths, both atoms feel different decelerating light forces at the beginning. Numerical simulations show a rapid redistribution

of the population among the m_F states during the first 10 μm, which leads to an asymmetry in the trap depth of the order of 3%. The net change of the trap depth due to statistical fluctuations of the number n of scattered photons and deviations from original straight-line trajectories due to anisotropy of the trapping potential [27, 33] scales as $n^{3/2}$ and is about 10% for the cooling laser intensities used in our measurements. The resulting predictions for the RE loss coefficient β_{RE} due to the uncertainties in the trap depth discussed above are shown in figure 11 (dashed lines). Although β_{RE} roughly reproduces our experimental data, the results have to be taken with care since the used GPM describes the RE loss processes qualitatively well but tends to underestimate the expected RE loss rates by about a factor of 1/5 as discussed in section 5.1. The included velocity distribution of the stored atoms in our calculations merely increases the RE loss coefficient by about 12%. So further studies are needed to explain this effect.

6. Conclusion

We have presented a detailed analysis of the cold collision measurements in a high-field gradient MOT. Two main effects result from the stiff magnetic field. The trap loading rate from the background gas, and thus the number of trapped atoms, is drastically reduced. Exact determination of the number of trapped atoms and monitoring its changes due to collisions in real time provide a novel tool for cold collision studies. The second effect of the strong magnetic fields is the reduced effective trap depth, which makes observation of hyperfine-changing ground-state collisions easier. We have observed and described theoretically a strong suppression of these collisions by the MOT repumping laser. This effect is always present in alkali MOTs and can mask measurements of β_{HCC}.

Acknowledgments

We thank S Gensemer, P Gould and E Hinds for valuable discussions. We furthermore wish to thank the Deutsche Forschungsgemeinschaft for support (ME 971/18).

Appendix. Background-gas collisions

In our experiment the loss rate $1/\tau_c$ for collisions with background gas is dominated by collisions with thermal Cs background atoms. This is not only shown experimentally by increasing the Cs background pressure and observing a proportional increase in both the loading rate R and loss rate $1/\tau_c$, as expected, but also by semiclassical calculations of the total loss cross section σ_{loss} due to small-angle scattering [34]. The collisional loss rate is given by $1/\tau_c = n_b \sigma_{loss} \tilde{v}_t$, where $\tilde{v}_t$ is the characteristic thermal velocity of the background atoms and $n_b = p/(k_B T)$ is the background-gas density. The main contribution to the total loss cross section σ_{loss} results from small scattering angles. In this case σ_{loss} is obtained by integrating the differential cross section within angles corresponding to a maximum energy transfer of $m\tilde{v}_t^2/2$ up to the trap depth. For our typical MOT parameters with a trap depth of $k_B \times 0.2$ K, $\tilde{v}_t = 237$ m s^{-1} and Cs background pressure $p = 10^{-10}$ mbar we obtain $1/\tau_c = 0.004$ s^{-1} for Cs–Cs collisions. The measured value is given by L_{1atom} for $N = 1$ and is observed to be of the same order of magnitude in all measurements. Note that an increase of the trap depth by a factor of 2 does not change σ_{loss} efficiently.

References

[1] Weiner J, Bagnato V S, Zilio S and Julienne P S 1999 *Rev. Mod. Phys.* **71** 1 and references therein
[2] Raab E L, Prentiss M, Cable A, Chu S and Pritchard D E 1987 *Phys. Rev. Lett.* **59** 2631

[3] Haubrich D, Höpe A and Meschede D 1993 *Opt. Commun.* **102** 225
[4] Höpe A, Haubrich D, Müller G, Kaenders W G and Meschede D 1993 *Europhys. Lett.* **22** 669
Höpe A 1994 *PhD Thesis* University of Hanover
[5] Willems P A, Boyd R A, Bliss J L and Libbrecht K G 1997 *Phys. Rev. Lett.* **78** 1660
[6] Ueberholz B, Kuhr S, Frese D, Meschede D and Gomer V 2000 *J. Phys. B: At. Mol. Opt. Phys.* **33** L135
[7] Gensemer S D, Sanchez-Villicana V, Tan K Y N, Grove T T and Gould P L 1997 *Phys. Rev.* A **56** 4055
[8] Lett P D, Phillips W D, Rolston S L, Tanner C E, Watts R N and Westbrook C I 1989 *J. Opt. Soc. Am.* B **6** 2084
[9] Drewsen M, Laurent P, Nadir A, Santarelli G, Clairon A, Castin Y, Grison D and Salomon C 1994 *Appl. Phys.* B **59** 283
[10] Townsend C G, Edwards N H, Cooper C J, Zetie K P, Foot C J, Steane A M, Szriftgiser P, Perrin H and Dalibard J 1995 *Phys. Rev.* A **52** 1423
[11] Mølmer K 1991 *Phys. Rev.* A **44** 5820
[12] Dalibard J, Reynaud S and Cohen-Tannoudji C 1984 *J. Phys. B: At. Mol. Phys.* **17** 4577
[13] Dalibard J and Cohen-Tannoudji C 1989 *J. Opt. Soc. Am.* B **6** 2023
[14] Wallace C D, Dinneen T P, Tan K Y N, Kumarakrishnan A, Gould P L and Javanainen J 1994 *J. Opt. Soc. Am.* B **11** 703
[15] Haubrich D, Schadwinkel H, Strauch F, Ueberholz B, Wynands R and Meschede D 1996 *Europhys. Lett.* **34** 663
[16] Gomer V, Strauch F, Ueberholz B, Knappe S and Meschede D 1998 *Phys. Rev.* A **58** R1657
[17] Gomer V, Ueberholz B, Knappe S, Strauch F, Frese D and Meschede D 1998 *Appl. Phys.* B **67** 689
[18] Walker T, Sesko D and Wieman C 1990 *Phys. Rev. Lett.* **64** 408
[19] Sesko D, Walker T, Monroe C, Gallagher A and Wieman C 1989 *Phys. Rev. Lett.* **63** 961
[20] Telles G D, Bagnato V S and Marcassa L G 2001 *Phys. Rev. Lett.* **86** 4496
[21] Gallagher A and Pritchard D E 1989 *Phys. Rev. Lett.* **63** 957
[22] Julienne P S and Vigué J 1991 *Phys. Rev.* A **44** 4464
[23] Walker T G, Sesko D W, Monroe C and Wieman C 1990 *The Physics of Electronic and Atomic Collisions (AIP Conf. Proc. vol 205)* ed A Dalgarno, R S Freund, P M Koch, M S Lubell and T B Lucatorto (New York: AIP) p 593
[24] Bali S, Hoffmann D and Walker T 1994 *Europhys. Lett.* **27** 273
[25] Sanchez-Villicana V, Gensemer S D, Tan K Y N, Kumarakrishnan A, Dinneen T P, Süptitz W and Gould P L 1995 *Phys. Rev. Lett.* **74** 4619
[26] Suominen K A 1996 *J. Phys. B: At. Mol. Opt. Phys.* **29** 5981
[27] Hoffmann D, Bali S and Walker T 1996 *Phys. Rev.* A **54** R1030
[28] Muniz S R, Marcassa L G S, Napolitano R, Telles G D, Weiner J, Zilio S C and Bagnato V S 1997 *Phys. Rev.* A **55** 4407
[29] Mott N F and Massey H S W 1965 *The Theory of Atomic Collisions* 3rd edn (Oxford: Clarendon)
[30] Marcassa L, Muniz S, de Queiroz E, Zilio S, Bagnato V S, Weiner J, Julienne P S and Suominen K A 1994 *Phys. Rev. Lett.* **73** 1911
[31] Su T and Bowers M T 1979 *Gas Phase Ion Chemistry* ed M T Bowers (London: Academic)
[32] Tang K T, Norbeck J M and Certain P R 1976 *J. Chem. Phys.* **64** 3063
[33] Ritchie N W M, Abraham E R I and Hulet R G 1994 *Laser Phys.* **4** 1066
Ritchie N W M, Abraham E R I, Xiao Y Y, Bradley C C, Hulet R G and Julienne P S 1995 *Phys. Rev.* A **51** R890
[34] Gomer V, Harms O, Haubrich D, Schadwinkel H, Strauch F, Ueberholz B, aus der Wiesche S and Meschede D 1997 *Hyperfine. Interact.* **109** 281